Environ. Sci. Technol. **2000**, *34,* 2479−2483

The Nature of Zn Precipitates Formed in the Presence of Pyrophyllite

ROBERT G. FORD* AND DONALD L. SPARKS

Department of Plant and Soil Sciences, University of Delaware, Newark, Delaware 19717

The partitioning of Zn to the pyrophyllite surface was studied as a function of surface loading for periods up to 4 months. Examination of the reaction products using X-ray absorption fine structure spectroscopy (XAFS) indicated the formation of a Zn precipitate at each surface loading. Comparison of the local structure of the surface precipitates to the structure of various hydroxide- and carbonate-bearing phases indicates the formation of a Zn−Al layered double hydroxide (LDH). The solubility of Zn following aging in pyrophyllite systems indicated that the initial Zn−Al LDH precipitates transformed to a more stable form. Increased Zn stability in these experimental systems may be attributed to an increase in LDH crystallinity (Ostwald ripening) or incorporation of Si within the LDH interlayer leading to transformation to a phyllosilicate-like phase. Our results support formation of an LDH precipitate as a precursor to Zn fixation in soils abundant in aluminosilicate minerals. These results augment recent findings that transition metals may form layered hydroxide and phyllosilicate-like precipitates during sorption to clay minerals. Acknowledgment of this process as a potential metal sequestration mechanism in certain soil types is important to assessment of contaminant attenuation. Development of a more comprehensive database of solubilities for these surface precipitates will facilitate more reliable estimates.

Introduction

Partitioning reactions (sorption) to clay mineral surfaces may control metal mobility in soils. Numerous studies have attempted to define the mechanisms by which metals partition from the soil solution to phyllosilicates (*1*−*3*). Electrostatic and chemical forces are considered to control sorption to the phyllosilicate surface. Electrostatic interactions are a result of the net negative structural charge developed within the phyllosilicate due to isomorphic substitutions or due to variable charge developed at hydroxyl edge sites (*4*). Hydroxyl edge sites may also scavenge metals from solution via specific chemical interactions to satisfy the unsaturated coordination environment of surface oxygen (*5*). However, recent studies that examined Ni sorption to a variety of phyllosilicates possessing a range of structural charge suggest that the formation of surface precipitates occurs under solution conditions undersaturated with respect to homogeneous precipitation of a pure hydroxide phase (*6, 7*). The surface precipitates have been identified as a mixed Ni−Al hydroxide-like phase, commonly referred to as a layered double hydroxide or LDH. It is proposed that the release of exchangeable or lattice Al from the phyllosilicate promotes the formation of an LDH (*7*−*9*).

An LDH is composed of sheets of edge-sharing metal octahedra separated by interlayer regions populated by anions. The structural formula is generally written, $[Me^{2+}_{1-x}Me^{3+}_{x}(OH)_2]^{x+}\cdot(x/n)A^{n-}\cdot mH_2O$, where the interlayer anion, A^{n-}, is required to neutralize the excess positive charge imparted by substitution of a trivalent cation into the brucite-like sheet (*10*). Examination of literature describing synthesis of LDH compounds suggests that many of the first row transition metals may be incorporated into the octahedral layer. Consistent with this expectation, the formation of LDH precipitates during Co sorption to Al-bearing oxides has also been observed (*9, 11, 12*). The observation of Ni− and Co−Al LDH formation suggests a potential sorption mechanism for other metals in soil or sediment environments with a significant fraction of weatherable Al-bearing minerals.

In an effort to examine the generality of this sorption mechanism to other metals, a study was performed to examine the long-term sorption of Zn to the clay mineral pyrophyllite. Numerous studies report incorporation of Zn into the LDH structure during preparation of catalyst starting materials (*10, 13*−*16*). Paulhiac and Clause (*11*) have also shown that a Zn−Al LDH forms during impregnation of γ-Al_2O_3 at pH 7.5 and a surface loading of approximately 26 000 mg kg^{-1}. However, recent studies that modeled Zn sorption to montmorillonite suggest that this metal primarily forms mononuclear adsorption complexes with surface functional groups or ion exchange sites (*17, 18*). The apparent lack of surface precipitate formation in these studies may have been limited by low surface loading (<6600 mg kg^{-1}), insufficient equilibration time for LDH nucleation, or competition with ion exchange sites (*19*). However, spectroscopic confirmation of sorbate speciation was not carried out in these studies.

Scheidegger et al. (*7*) showed that Ni surface precipitate nucleation was slower on montmorillonite than pyrophyllite. A time-resolved XAFS spectroscopic study indicated nucleation times of minutes versus days at a surface loading of 17 600 mg kg^{-1} for pyrophyllite and montmorillonite, respectively. Recent studies indicated that the extent of Al release limits the rate of Ni− and Co−Al LDH formation on kaolinite (*9, 20*). Studies examining Zn sorption to montmorillonite showed increased immobilization of Zn when montmorillonite exchange sites were saturated with mononuclear or polynuclear Al species (*21*). These experiments were carried out at relatively low surface loading (3270 mg kg^{-1}), but the systems were allowed to age up to 60 weeks. Lothenbach et al. (*21*) showed that immobilization was significant for Ni and Zn, but not for Cd and Pb. These macroscopic results are consistent with nucleation of Ni− and Zn−Al LDH phases over long equilibration periods. Thus, the limiting factors governing Zn−Al LDH formation during sorption to Al-bearing minerals appear to be a sufficient supply of labile Al and contact times sufficient to allow precipitate nucleation.

This work extends the investigations examining the formation of metal surface precipitates at the pyrophyllite surface to include Zn. The goal was to assess the potential for LDH formation over a range of surface loading. XAFS spectroscopy was used to characterize Zn surface precipitates formed over aging periods of weeks to months. The apparent

* Corresponding author phone: (580)436-8872; fax: (580)436-8703; e-mail: ford.robert@epa.gov. Current address: Robert S. Kerr Environmental Research Center, U.S. EPA, P.O. Box 1198, Ada, OK 74820.

10.1021/es991330q CCC: $19.00
Published on Web 05/02/2000

solubility of the surface precipitates was compared to the solubility of known hydroxide- and carbonate-bearing precipitates to assess the potential importance of LDH formation for Zn sequestration in soils.

Methods and Materials

The sorption of Zn to the clay mineral, pyrophyllite, was studied over time in batch systems. Stock 10 g L^{-1} suspensions of the <2 μm size fraction of pyrophyllite were aged in 0.1 M $NaNO_3$ at pH 7.5 for 2 months prior to contact with dissolved Zn. Aliquots of the preequilibrated solids were then diluted to 5 g L^{-1} in sorption experiments. The pH was buffered by addition of 4-(2-hydroxyethyl)-1-piperazineethanesulfonic acid (HEPES) at a final concentration of 50 mM. The pK_a of HEPES is 7.5 at 25 °C. Previous studies showed that HEPES does not interfere with transition metal sorption to mineral surfaces (*22*). Prior to Zn addition, the pH was adjusted to 7.5 with 0.1 M NaOH. Zinc was then introduced into the suspension by adding the appropriate volume of a 0.075 M $Zn(NO_3)_2$ solution to provide a final concentration ranging from 0.1 to 0.8 mM Zn. Solubility calculations indicated that Zn was oversaturated with respect to precipitation only in systems containing 0.8 and 0.4 mM Zn based on measured aqueous Zn concentration. These systems were initially oversaturated with respect to Zn−Al LDH, $ZnCO_3$, $Zn_5(OH)_6(CO_3)_2$, and the nitrate-form of $Zn_5(OH)_8Cl_2$ (see Supporting Information). The ionic strength of the suspension was set at 0.1 M, accounting for contributions from $NaNO_3$, HEPES, and Na^+ from base additions. The pH varied < 0.05 pH units during the sorption experiment. Samples (5 mL) were periodically collected from the suspension and filtered through a 0.2 μm membrane filter. Filtered supernatants were analyzed for dissolved Zn and Si by atomic absorption/emission spectroscopy.

Solid samples were collected periodically for characterization using XAFS spectroscopy. Solids were isolated from suspension under vacuum filtration and the wet paste was transferred to an aluminum holder. The paste was sealed into the holder with 0.0005-in. thick Kapton polymide tape (CHR Industries, type K-104) to avoid moisture loss during analysis. XAFS measurements were carried out at beamline X-11A at the National Synchrotron Light Source, Brookhaven National Laboratory. In addition, data were collected in fluorescence mode for a synthetic Zn−Al LDH diluted to 1% w/w in boron nitride. The LDH phase was synthesized at pH 6.3 and an initial Zn:Al ratio of 3:1 using the method of Taylor (*23*). The final precipitate had a Zn:Al mole ratio of 1.7 based on total dissolution of the solid and measurement of dissolved Zn and Al by atomic absorption spectroscopy.

The raw XAFS data were processed using standard procedures (*24*). Briefly, the k^3-weighted $\chi(k)$ function was Fourier transformed over the range 1.2−13.5 $Å^{-1}$. Single and multishell fits were carried out using WinXAS97 1.0 (*25*) and Zn−O, Zn−Zn, and Zn−Al scattering paths generated by FEFF6 (*26*) from the refinement of a Mg−Al hydrotalcite (*27*). Zinc was substituted for Mg in the structure, since both atoms have similar radii (*28*). An estimate of the amplitude reduction factor, S_o^2, was determined by fitting the raw fluorescence data for a synthetic Zn−Al LDH. Multishell fitting using Zn−O, Zn−Zn, and Zn−Al paths resulted in a value of approximately 0.9 for S_o^2 when the first-shell Zn−O coordination number, CN_{Zn-O}, was fixed at 6. Zinc is octahedrally coordinated to oxygen atoms within the LDH structure (*29, 30*). During EXAFS spectroscopic fits of the sorption samples, S_o^2 was fixed at 0.9. Initial fits to the first shell of the Zn-pyrophyllite samples indicated that Zn was predominantly coordinated to O in an octahedral environment in all cases ($CN_{Zn-O} = 6.01 \pm 0.2$; $2.03 \leq R_{Zn-O} \leq 2.06$). Subsequently, multishell fits were carried out using either a combination of (1) Zn−O, Zn−Zn or (2) Zn−O, Zn−Zn, Zn−Al paths.

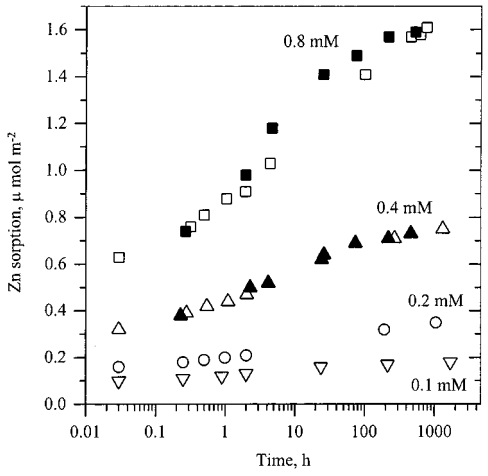

FIGURE 1. Partitioning of Zn to pyrophyllite for total Zn concentrations ranging from 0.1 to 0.8 mM as a function of aging time in batch systems. Replicate experiments were run for systems with 0.4 and 0.8 mM as shown by closed and open symbols. Experimental conditions: pH 7.5, 5 g L^{-1} pyrophyllite, and 0.1 M ionic strength.

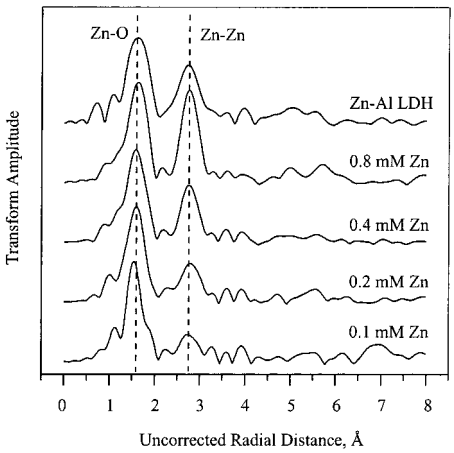

FIGURE 2. RSFs derived from EXAFS data for a synthetic Zn−Al LDH and Zn-pyrophyllite samples aged for periods of 387−2982 h. The first peak is associated with the first-shell Zn−O bond, and the second peak is associated with the second-shell Zn−Zn and Zn−Al coordination environment.

Results and Discussion

The partitioning of Zn to pyrophyllite as a function of time is shown in Figure 1. The results show an initial rapid Zn uptake within the first 5 min. In all cases, Zn uptake was continuous throughout the entire equilibration period, and all systems approached complete partitioning of Zn to the solid phase. Replicate experiments at 0.8 and 0.4 mM total Zn indicated that the sorption behavior was reproducible. Silica was released from pyrophyllite during equilibration, indicating partial dissolution of the pyrophyllite surface (data not shown). This behavior was consistent with that shown in previous research examining Ni and Co partitioning to a variety of clay minerals (*6−9, 12*). Spectroscopic characterization of the sorption product indicated that an LDH formed at the mineral−water interface, where Al was derived from the sorbent phase.

Solids from the Zn-pyrophyllite systems were collected for XAFS characterization after aging periods ranging from 387 to 2982 h. Radial structure functions (RSF) are shown in Figure 2 for sorption samples and a synthetic Zn−Al LDH. There are two predominant peaks apparent in the RSF for each sorption sample and the synthetic precipitate. For sorption samples, the intensity of the second-shell peak

TABLE 1. Results of Fitting EXAFS Data for Zn−Al LDH Precipitate and Zn-Pyrophyllite Sorption Samples

fit method[a]	Zn loading,[b] mg kg^{-1}	aging time, h	Zn−O, Å	CN	σ^2 [c]	Zn−Zn Zn−Al, Å	CN	σ^2	ΔE_0[d]	reduced χ^2 [e]
two shell	Zn−Al LDH		2.07	6.3	0.009	3.10	3.8	0.009	0.537	99.7
three shell			2.07	6.0	0.010	3.08	4.3	0.010	0.003	53.7
						3.06	2.4	0.010		
two shell	10 180	531	2.06	6.2	0.010	3.10	3.1	0.006	0.654	182.7
three shell	(0.8 mM)		2.06	6.1	0.009	3.10	3.5	0.007	0.441	138.3
						3.09	1.0	0.007		
two shell	4629	387	2.04	6.1	0.011	3.10	1.9	0.011	0.391	222.3
three shell	(0.4 mM)		2.04	5.9	0.011	3.09	2.7	0.007	0.074	128.2
						3.10	1.4	0.007		
two shell	2243	2982	2.03	5.7	0.010	3.09	1.6	0.007	0.215	743.3
three shell	(0.2 mM)		2.03	5.5	0.010	3.08	3.2	0.009	0.313	386.7
						3.11	2.5	0.009		
two shell	1154	2143	2.02	5.8	0.011	3.09	1.1	0.006	0.171	589.8
three shell	(0.1 mM)		2.02	5.6	0.010	3.07	2.5	0.008	0.359	435.2
						3.09	2.5	0.008		

[a] Two shell: RSF was fit using Zn−O and Zn−Zn for the first and second shells, respectively, and S_0^2 was fixed at 0.9. Three shell: The RSF was fit using Zn−O for the first shell and both Zn−Zn and Zn−Al for the second shell. S_0^2 was fixed at 0.9 and σ^2 was set equal for Zn−Zn and Zn−Al scattering paths. [b] The Zn−Al LDH was a synthetic precipitate used as a structural reference. For sorption samples, the total aqueous Zn concentration is listed in parentheses. [c] Debye−Waller factor. [d] Energy shift; constrained to be equal for each shell. [e] Reduced $\chi^2 = \chi^2$/(total number of data points − fit parameters).

decreased as the total Zn surface loading decreased. Results from fitting the XAFS data are presented in Table 1. For each sample, the fit quality was evaluated using two fitting scenarios: (1) Zn−O first shell in combination with second-shell Zn−Zn and (2) Zn−O first shell in combination with Zn−Zn and Zn−Al scattering paths in the second shell. In general, fits of the first shell indicated that Zn was predominantly in an octahedral environment. There was an apparent decrease in the distance of the Zn−O scattering path with a decrease in Zn surface loading. The Zn−O bond distance decreased from 2.06 to 2.02 Å as the Zn surface loading decreased from 10 180 to 1154 mg kg^{-1}. In all cases, the inclusion of a Zn−Al scattering path improved the overall fit to the RSF as indicated by a decrease for the value of the reduced χ^2. The Zn:Al ratio determined by XAFS for the Zn−Al LDH was 1.8, which was in close agreement with the ratio determined by dissolution of the solid (Zn:Al = 1.7). The fit results for the synthetic Zn−Al LDH and the Zn-pyrophyllite sorption samples indicate that an LDH surface precipitate formed during Zn partitioning from solution to the pyrophyllite surface with aging.

In general, previous studies employing XAFS demonstrate that Zn occupies an octahedral environment within the layered LDH structure (*29*, *30*). The Zn−O bond distances resulting from XAFS fits to the experimental data are consistent with this interpretation. The observed decrease in the Zn−O bond distance with decreased surface loading is consistent with a decrease in the Zn:Al ratio from approximately 3.5 to 1.0 for the second-shell XAFS fit. Bellotto et al. (*27*) have shown by powder X-ray diffraction structure refinements of Mg−Al LDH precipitates that the Mg−O distance decreases from 2.04 to 2.01 Å as the Mg:Al ratio decreases from 5 to 1. While the Zn:Al ratio derived from XAFS provides only a rough estimate due to associated error, it is consistent with expectations. For the Zn−Al LDH and the Zn-pyrophyllite samples, Zn−Zn and Zn−Al second-shell bond distances on the order of 3.06−3.11 Å can be attributed to an edge-sharing local structure. However, in addition to Zn−Al LDH, this feature is shared by other potential phases.

The local structure is listed in Table 2 for precipitate phases that could have formed in these experiments, based on the composition of the aqueous solution. The bond distances were calculated using ATOMS and FEFF6 based on published X-ray structure refinements (*27*, *31*−*35*). The formation of ϵ-$Zn(OH)_2$ can be ruled out, because both Zn−O and Zn−Zn distances differ significantly from those obtained for the sorption samples. The bond distances in ϵ-$Zn(OH)_2$ are due to Zn residing exclusively in a tetrahedral environment (*35*). The formation of carbonate bearing Zn precipitates could potentially have occurred, because CO_2 was not excluded from the experimental systems. However, XAFS data indicate that the formation of smithsonite and hydrozincite did not occur based on measured Zn−Zn and Zn−O bond distances. For smithsonite, Zn−Zn bond distances are a result of Zn octahedra sharing corners, which results in a much larger bond distance than an edge-sharing configuration (*34*). The formation of hydrozincite can also be excluded due to the absence of a Zn−Zn bond distance between 3.53 and 3.60 Å, which results from corner sharing of a Zn tetrahedron and a Zn octahedron (*31*). Of the Zn precipitates listed in Table 2, only the Zn−Al LDH and $Zn_3(OH)_4(NO_3)_2$ phases share a common short-range order structure that is consistent with our Zn-pyrophyllite sorption samples. However, given the large range of Zn−O bond distances predicted for $Zn_3(OH)_4(NO_3)_2$, a larger first-shell Debye−Waller factor is anticipated. Thus, based on XAFS results, identification of the precipitates forming in Zn-pyrophyllite systems as a Zn−Al LDH appears the most likely conclusion.

TABLE 2. Bond Distances for First-Shell Zn−O and Second-Shell Zn−Zn Environments in Potential Precipitate Phases[e]

solid phase	Zn−O, Å	Zn−Zn, Å	ref
ϵ-$Zn(OH)_2$, wulfingite	1.94−1.97 (T)[a]	3.40−3.41 (T_C)	(*35*)
$ZnCO_3$, smithsonite	2.11 (O)	3.67 (O_C)	(*34*)
$Zn_5(OH)_6(CO_3)_2$,	1.85−1.99 (T)	3.53−3.60 (TO_C)	(*31*)
hydrozincite	2.04−2.16 (O)	2.99−3.29 (O_E)	
$Zn_3(OH)_4(NO_3)_2$	1.82−2.45 (O)	3.10−3.13 (O_E)	(*33*)
$Zn_5(OH)_8(NO_3)_2{\cdot}2H_2O$	1.95 (T)	3.42−3.64 (TO_C)	(*32*)
	2.02−2.19 (O)	3.10−3.16 (O_E)	
Zn−Al LDH[b]	2.01 (O)[c]	3.05 (O_E)[c]	(*27*)
	2.04 (O)[d]	3.08 (O_E)[d]	

[a] Notation: T, tetrahedral; O, octahedral; T_C, corner-sharing tetrahedra; O_C, corner-sharing octahedra; O_E, edge-sharing octahedra; TO_C, corner-sharing octahedron-tetrahedron. [b] Based on substitution of Zn for Mg in a hydrotalcite structure. [c] Mg:Al = 2:1. [d] Mg:Al = 5:1. [e] Distances were calculated using ATOMS and FEFF6 with atomic positions derived from X-ray structure refinement. The amplitude reduction factor, S_0^2, and the Debye−Waller term, σ^2, were set to 1.0 and 0.0, respectively, during modeling.

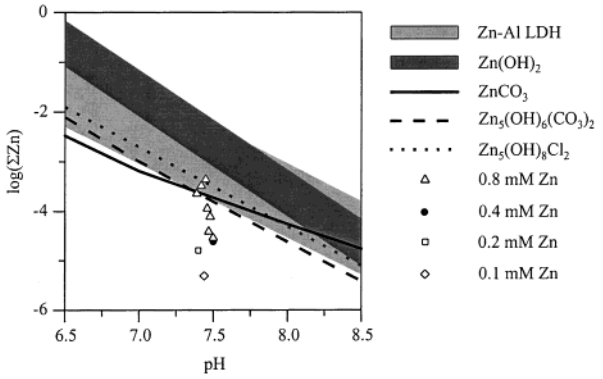

FIGURE 3. Zn solubility fields for potential hydroxide- and carbonate-bearing precipitates. Total soluble Zn concentration, ΣZn, is plotted on the ordinate. The concentration of soluble Zn in equilibrium with reference precipitates was estimated using the TJ equation for activity coefficient estimation with 0.1 M ionic strength and assuming that Zn^{2+} was the dominant species. The stability region for the Zn−Al LDH was bounded by a Cl^- activity 1 to 100 mM. The stability region for $Zn(OH)_2$ was based on the solubility of the least and most stable forms, α-$Zn(OH)_2$ and ϵ-$Zn(OH)_2$, respectively. Zn solubility for carbonate-bearing phases was based on 10^{-3} M total inorganic carbon. Aqueous Zn activities are plotted from Zn-pyrophyllite experiments. The complete aging series is shown for the experiment with a total Zn concentration of 0.8 mM, where log(ΣZn) decreased with time. Only the final total Zn concentration is shown for experiments with 0.4, 0.2, and 0.1 mM total added Zn. However, the range in log(ΣZn) for these systems was −3.6 to −4.6, −3.9 to −4.8, and −4.3 to −5.3, respectively.

This analysis is supported by comparison of the Zn solubility in aged Zn-pyrophyllite systems compared to the concentration of Zn in equilibrium with the phases listed in Table 2. The results of these calculations are shown in Figure 3 (additional details are available in the Supporting Information). The solubility of Zn as a function of pH is shown for several poorly crystalline and crystalline phases. The solubility relationships for α-$Zn(OH)_2$, ϵ-$Zn(OH)_2$, $ZnCO_3$, $Zn_5(OH)_6(CO_3)_2$, and $Zn_5(OH)_8Cl_2$ were taken from the MINTEQA2 database (*36*). Results for $Zn_5(OH)_8Cl_2$ are plotted, because thermodynamic constants are not available for the nitrate form. However, both the nitrate- and chloride-form of this phase share the same basic structure (*33*). In addition, predictions for the chloride-form of $Zn_3(OH)_4(NO_3)_2$ are not shown since Zn solubility is greater for this phase (*36*). The solubility range shown for Zn−Al LDH was developed using the relationship reported by Boclair and Braterman (*37*) for a freshly precipitated chloride-form of a Zn−Al LDH. The solubility band shown was calculated based on equilibrium with solutions containing 0.1 to 100 mM Cl. It was assumed that the difference in Zn solubility for the nitrate- or chloride-form of Zn−Al LDH was insignificant. This assumption was partly supported by the similarity in exchangeability of these anions from the LDH interlayer (*10, 38, 39*).

Comparison of predicted Zn solubility for the phases shown in Figure 3 indicated that under the conditions of the sorption experiment, i.e., pH 7.5 and 0.1 M ionic strength, a poorly crystalline Zn−Al LDH was more stable than the crystalline ϵ-$Zn(OH)_2$ or the hydroxy-chloride. If it is assumed that the experimental solutions were in equilibrium with atmospheric CO_2, then equilibrium calculations suggest that smithsonite or hydrozincite could compete with Zn−Al LDH formation (Figure 3). However, measured Zn concentrations in Zn-pyrophyllite systems show that Zn solubility continued to drop below that of a poorly crystalline Zn−Al LDH and other hydroxide- or carbonate-bearing phases. For example, the Zn concentration for the 0.8 mM total Zn experimental system started within the range predicted for a poorly crystalline Zn−Al LDH phase. However, with time the Zn concentration decreased below that predicted for all phases shown. This behavior was exhibited for all total Zn concentrations studied. Thus, while initial formation of a poorly crystalline Zn−Al LDH in Zn-pyrophyllite systems was possible based on solubility considerations, this does not represent the equilibrium endpoint.

There are two possible explanations for the observed decrease in Zn solubility with aging. As shown by Ford et al. (*40*), the overall stability of an LDH surface precipitate may increase over time due to exchange of silica for nitrate within the LDH interlayer. This phenomenon is supported by research that showed incorporation of silica into the interlayer of a Zn−Al LDH leading to the formation of a more stable phyllosilicate-like phase (*14*). For these experimental systems, interlayer silica exchange could be driven by the slow dissolution of pyrophyllite. Thompson et al. (*41*) showed that incorporation of silica within the interlayer of a Co−Al LDH may lead to a two-order-of-magnitude reduction in Co solubility.

Another possible explanation for a decrease in the Zn solubility is an increase of the crystallinity of the Zn−Al LDH precipitate due to Ostwald ripening (*42*). It is not possible to assess the influence of an improvement in Zn−Al LDH crystallinity due to a lack of solubility data for a well-crystallized phase. Comparison of solubility estimates for a poorly crystalline (*37*) and a crystalline (*41*) Co−Al LDH indicates more than an order-of-magnitude decrease in the solubility of the divalent metal. Thus, the observed reduction in Zn solubility during aging may be due to an increase in LDH crystallinity as well as a gradual transformation to a phyllosilicate-like phase.

The results of these experimental systems support recent observations that divalent metals within the first transition metal series may form LDH phases during sorption to Al-bearing minerals. Measurements of Zn solubility suggested that the initially formed LDH phase was metastable. One potential endpoint is the ultimate formation of a phyllosilicate-like phase. This hypothesis was supported, in part, by previous observations that Zn phyllosilicates form from solution over time at ambient temperature when sufficient levels of dissolved silica and/or Al are available (*43−46*). These studies suggest that formation of a phyllosilicate-like phase may be a viable endpoint for Zn partitioning to clay surfaces under natural settings. However, the extent of this process will depend on the relative percentage of competing surfaces such as iron (hydr)oxides. These results in combination with previous studies highlight the need for a more comprehensive thermodynamic database for LDH phases that can serve as metastable precursors to more stable phases. This information will help guide assessments of the long-term stability of metals such as Co, Ni, and Zn that partition to clay surfaces in soils and sediments.

Acknowledgments

Supported by grants from the USDA-NRI Program, the DuPont Company, and the Delaware Research Partnership Program. This manuscript benefited from comments by Dr. Rick Wilkin, Ms. Amy Bryce, and three anonymous, constructive reviews. Although R.G.F. is employed by the U.S. Environmental Protection Agency, this manuscript has not been subjected to Agency review and therefore does not necessarily reflect the views of the Agency, and no official endorsement should be inferred.

Supporting Information Available

Calculations and solubility data used to generate Figure 3. This material is available free of charge via the Internet at http://pubs.acs.org.

Literature Cited

(1) Brown, G. E., Jr.; Parks, G. A.; O'Day, P. A. In *Mineral Surfaces*; Vaughan, D. J., Pattrick, R. A. D., Eds.; Chapman & Hall: London, 1995; Vol. 5, p 129.
(2) Scheidegger, A. M.; Sparks, D. L. *Soil Sci.* **1996**, *161*, 813.
(3) Brown, G. E. Jr.; Henrich, V. E.; Casey, W. H.; Clark, D. L.; Eggleston, C.; Felmy, A.; Goodman, D. W.; Gratzel, M.; Maciel, G.; McCarthy, M. I.; Nealson, K. H.; Sverjensky, D. A.; Toney, M. F.; Zachara, J. M. *Chem. Rev.* **1999**, *99*, 77.
(4) Sparks, D. L. *Environmental Soil Chemistry*; Academic Press: San Diego, 1995.
(5) Sposito, G. *The Surface Chemistry of Soils*; Oxford University Press: New York, 1984.
(6) Scheidegger, A. M.; Lamble, G. M.; Sparks, D. L. *J. Colloid Interface Sci.* **1997**, *186*, 118.
(7) Scheidegger, A. M.; Strawn, D. G.; Lamble, G. M.; Sparks, D. L. *Geoch. Cosmochim. Acta* **1998**, *62*, 2233.
(8) Scheinost, A. C.; Ford, R. G.; Sparks, D. L. *Geoch. Cosmochim. Acta* **1999**, *63*, 3193.
(9) Thompson, H. A.; Parks, G. A.; Brown, G. E., Jr. *Geoch. Cosmochim. Acta* **1999**, *63*, 1767.
(10) Cavani, F.; Trifiro, F.; Vaccari, A. *Catal. Today* **1991**, *11*, 173.
(11) Paulhiac, J. L.; Clause, O. *J. Am. Chem. Soc.* **1993**, *115*, 11602.
(12) Towle, S. N.; Bargar, J. R.; Brown, G. E.; Parks, G. A. *J. Colloid Interface Sci.* **1997**, *187*, 62.
(13) Thevenot, F.; Szymanski, R.; Chaumette, P. *Clays Clay Miner.* **1989**, *37*, 396.
(14) Depege, C.; El Metoui, F.-Z.; Forano, C.; de Roy, A.; Dupuis, J.; Besse, J.-P. *Chem. Mater.* **1996**, *8*, 952.
(15) Puttaswamy, N. S.; Kamath, P. V. *J. Mater. Chem.* **1997**, *7*, 1941.
(16) Velu, S.; Ramkumar, V.; Narayanan, A.; Swamy, C. S. *J. Mater. Sci.* **1997**, *32*, 957.
(17) Bradbury, M. H.; Baeyens, B. *J. Cont. Hydr.* **1997**, *27*, 223.
(18) Bradbury, M. H.; Baeyens, B. *Geoch. Cosmochim. Acta* **1999**, *63*, 325.
(19) Elzinga, E. J.; Sparks, D. L. *J. Colloid Interface Sci.* **1999**, *213*, 506.
(20) Eick, M. J.; Fendorf, S. E. *Soil Sci. Soc. Am. J.* **1998**, *62*, 1257.
(21) Lothenbach, B.; Furrer, G.; Schulin, R. *Environ. Sci. Technol.* **1997**, *31*, 1452.
(22) Nowack, B.; Sigg, L. *J. Colloid Interface Sci.* **1996**, *177*, 106.
(23) Taylor, R. M. *Clay Miner.* **1984**, *19*, 591.
(24) Brown, G. E. Jr.; Calas, G.; Waychunas, G. A.; Petiau, J. In *Spectroscopic Methods in Mineralogy and Geology*; Hawthorne, F. C., Ed.; Mineralogical Society of America: Washington, DC, 1988; Vol. 18, p 431.
(25) Ressler, T. *J. Phys. IV* **1997**, *7*, 269.
(26) Zabinsky, S. L.; Rehr, J. J.; Ankudinov, A.; Albers, R. C.; Eller, M. J. *Phys. Rev. B* **1995**, *52*, 2995.
(27) Bellotto, M.; Rebours, B.; Clause, O.; Lynch, J.; Bazin, D.; Elkaim, E. *J. Phys. Chem.* **1996**, *100*, 8527.
(28) Shannon, R. D. *Acta Crystallogr.* **1976**, *A32*, 751.
(29) Evans, J.; Pillinger, M.; Zhang, J. *J. Chem. Soc., Dalton Trans.* **1996**, *14*, 2963.
(30) Porta, P.; Morpurgo, S.; Pettiti, I. *J. Solid State Chem.* **1996**, *121*, 372.
(31) Ghose, S. *Acta Crystallogr.* **1964**, *17*, 1051.
(32) Stahlin, W.; Oswald, H. R. *Acta Crystallogr.* **1970**, *B26*, 860.
(33) Louer, P. M.; Louer, D.; Grandjean, D. *Acta Crystallogr.* **1973**, *B29*, 1696.
(34) Effenberger, H.; Mereiter, K.; Zemann, J. *Z. Kristallogr.* **1981**, *156*, 233.
(35) Stahl, R.; Jung, C.; Lutz, H. D.; Kockelmann, W.; Jacobs, H. *Z. Anorg. Allg. Chem.* **1998**, *624*, 1130.
(36) Allison, J. D.; Brown, D. S.; Novo-Gradac, K. J. *MINTEQA2/PRODEFA2, A Geochemical Assessment Model for Environmental Systems: Version 3.0 User's Manual*; United States Environmental Protection Agency: Athens, GA, 1991.
(37) Boclair, J. W.; Braterman, P. S. *Chem. Mater.* **1999**, *11*, 298.
(38) Bish, D. L. *Bull. Mineral.* **1980**, *103*, 170.
(39) Badreddine, M.; Khaldi, M.; Legrouri, A.; Barroug, A.; Chaouch, M.; de Roy, A.; Besse, J. P. *Mater. Chem. Phys.* **1998**, *52*, 235.
(40) Ford, R. G.; Scheinost, A. C.; Scheckel, K. G.; Sparks, D. L. *Environ. Sci. Technol.* **1999**, *33*, 3140.
(41) Thompson, H. A.; Parks, G. A.; Brown, G. E., Jr. *Clays Clay Miner.* **1999**, *47*, 425.
(42) Morse, J. W.; Casey, W. *Am. J. Sci.* **1988**, *288*, 537.
(43) Faust, G. T. *Am. Mineral.* **1951**, *36*, 795.
(44) Tiller, K. G.; Pickering, J. G. *Clays Clay Miner.* **1974**, *22*, 409.
(45) Harder, H. *Clay Miner.* **1977**, *12*, 281.
(46) Leggett, G. E. *Soil Sci. Soc. Am. J.* **1978**, *42*, 262.

Received for review December 1, 1999. Revised manuscript received March 20, 2000. Accepted March 20, 2000.

ES991330Q